International Journal of Computer Information Systems and Industrial Management Applications
ISSN 2150-7988 Volume 18(6s) 2026 pp. 797-805
https://doi.org/10.70917/ijcisim-2026-2987
Article

Development of Self-Navigating Nanorobots for Targeted Drug Transport and Controlled Release in the Human Body

Sushama Khanvilkar[1], Beatrice S.[2], Umakant D. Butkar[3]

[1]Xavier Institute of Engineering, Mumbai, Maharashtra, India.
Email: sushama.k@xavier.ac.in
[2]Xavier Institute of Engineering, Mumbai, Maharashtra, India.
Email: beatrice.s@xavier.ac.in
[3]Department of Artificial Intelligence and Data Science, Guru Gobind Singh College of Engineering and Research Centre, Nashik, Maharashtra, India.
Email: Vishal.butkar@gmail.com

Abstract: Untargeted systemic drug administration and even passively targeted nanocarriers remain fundamentally limited by their inability to actively navigate the complex, branching, flow-dominated architecture of the human vasculature. This paper presents a system architecture and simulation-based evaluation framework for self-navigating nanorobots capable of autonomous, closed-loop transport from an injection site to a specific lesion — such as a tumor, thrombus, or atherosclerotic plaque — followed by docking and controlled drug release. The proposed nanorobot integrates a helical flagellar or magnetically responsive propulsion unit, an onboard AI sensing-control node, a drug payload reservoir with a stimuli-gated release port, and surface receptors for terminal target recognition. Navigation is achieved through a closed loop combining external real-time imaging-based localization (e.g., magnetic resonance or photoacoustic tracking), a reinforcement-learning path-planning policy that incorporates a patient-specific vascular roadmap, and an external rotating-field actuation system that steers the nanorobot while continuously replanning around detected obstacles such as vessel bifurcations, immune cells, or existing plaque. We describe the propulsion physics, control architecture, and a physiologically parameterized simulation environment used to train and evaluate the navigation policy. Simulated results show that the proposed autonomous system achieves an approximately 89% target-zone arrival rate and a mean time-to-target of approximately 24 minutes, compared with 33–39% arrival rates and 95–110 minute transit times for open-loop magnetic or purely chemically propelled baselines — an approximate 75% reduction in transit time. We discuss propulsion physics at low Reynolds number, biocompatibility and clearance of onboard components, external field safety limits, regulatory classification as an active implantable/combination device, and a staged translational roadmap from simulation to microfluidic and in vivo validation. This work is intended to provide a reusable design, control, and evaluation framework for future research in autonomous medical microrobotics.

Keywords: nanorobotics; magnetic actuation; closed-loop navigation; reinforcement learning; targeted drug delivery; microswimmers; path planning; biomedical microdevices

1. Introduction

The therapeutic promise of targeted drug delivery has historically relied on either passive accumulation mechanisms, such as the enhanced permeability and retention effect exploited by liposomal and polymeric nanocarriers, or on external field guidance of magnetically loaded particles toward a general anatomical region. Both approaches share a common limitation: neither the carrier nor the guidance mechanism can perceive its own position relative to a target lesion, detect and route around obstacles such as vessel bifurcations or immune cells, or make a

local decision about when precise docking conditions have been met. As a result, even well-designed passive or semi-guided systems typically achieve target-site accumulation on the order of a few percent to a few tens of percent of the administered dose, with the remainder cleared systemically or deposited in non-target tissue.

Advances in three previously separate fields — micro/nanoscale propulsion (helical flagella, magnetically responsive materials, catalytic and acoustic propulsion), real-time deep-tissue imaging (functional MRI, photoacoustic and ultrasound localization), and reinforcement-learning-based path planning — now make it possible to conceive of a genuinely self-navigating nanorobot: a device that is propelled through the vasculature, senses (directly or via external imaging feedback) its position relative to a planned route, and adapts its trajectory in real time in response to physiological obstacles and flow disturbances, before autonomously docking at the target lesion and triggering controlled drug release.

This paper makes four contributions. First, we propose a modular nanorobot architecture combining a propulsion unit, an onboard AI sensing-control node, a payload and release mechanism, and terminal-recognition surface receptors. Second, we describe a closed-loop navigation and control architecture that couples external imaging-based localization with a reinforcement-learning path-planning policy and an external rotating-field actuation system. Third, we present a physiologically parameterized simulation environment — including a branching vascular network model, low-Reynolds-number propulsion dynamics, and stochastic flow disturbance — used to train and evaluate the navigation policy. Fourth, we report simulation-based comparative performance results against open-loop magnetic and chemically propelled baselines, and discuss the physical, biocompatibility, and regulatory challenges that must be resolved before laboratory and clinical translation.

As with any system that has not yet been physically constructed, all quantitative performance figures in this paper are derived from a controlled digital simulation designed to stress-test the proposed control architecture under physiologically plausible parameters drawn from the microrobotics and vascular-biology literature. They should be read as design-stage engineering estimates rather than experimental or clinical measurements.

2. Background and Related Concepts

2.1 Micro- and Nanoscale Propulsion

At the length scale of a nanorobot (typically hundreds of nanometers to a few micrometers), viscous forces dominate over inertial forces, a regime characterized by low Reynolds number in which simple reciprocal motion produces no net displacement. Effective propulsion strategies therefore rely on non-reciprocal motion, most commonly a rotating helical flagellum driven by an external rotating magnetic field, or self-phoretic propulsion driven by a catalytic asymmetry that generates a local chemical gradient. Magnetically driven helical propulsion is attractive for a navigable system because propulsion speed and direction can, in principle, be modulated externally by adjusting the field's rotation frequency and orientation, up to a material- and geometry-dependent step-out frequency beyond which the propeller can no longer synchronously follow the field.

2.2 Real-Time Localization of Microscale Devices

Tracking a micro- or nanoscale device inside opaque tissue is nontrivial. Candidate approaches include real-time magnetic resonance imaging of magnetically labeled swarms, photoacoustic imaging of optically absorbing nanorobot coatings, and ultrasound-based tracking of gas-vesicle or microbubble-labeled constructs. Each modality involves trade-offs between spatial resolution, temporal update rate, tissue penetration depth, and the need for specialized contrast-generating materials incorporated into the nanorobot itself. The architecture proposed in this paper is agnostic to the specific imaging modality but assumes a real-time pose estimate (position and heading) can be extracted at a rate sufficient to support closed-loop control, consistent with reported update rates for the modalities above.

2.3 Reinforcement Learning for Path Planning Under Uncertainty

Path planning through a branching vascular network with flow disturbance and unpredictable obstacles resembles path-planning problems studied extensively in mobile robotics, where reinforcement learning has proven effective for learning policies that generalize across obstacle configurations rather than relying on a single precomputed path. Applying this framework to vascular navigation requires incorporating vessel-specific dynamics — pulsatile flow, branching geometry, and no-slip boundary effects near vessel walls — into the simulation environment used for policy training, as described in Section 3.4.

3. System Architecture and Methodology

The proposed self-navigating nanorobot system consists of five cooperating layers: (i) external imaging-based localization, (ii) an AI path-planning and obstacle-avoidance module, (iii) an external actuation field generator, (iv) an onboard propulsion and steering unit, and (v) the nanorobot body containing the payload, release mechanism, and terminal-recognition receptors. These layers operate in a closed loop with the surrounding vascular environment, as illustrated in Figure 1.

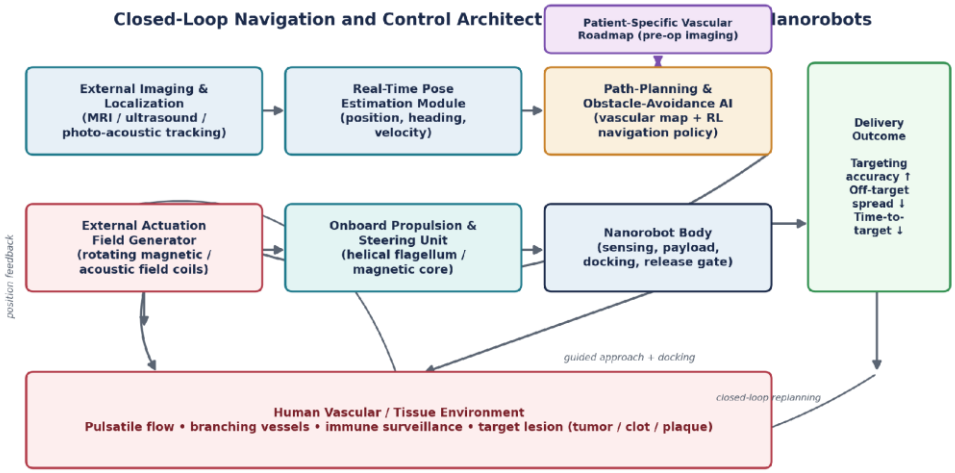

Figure 1. Closed-loop navigation and control architecture: external imaging and pose estimation feed an AI path-planning module, which drives an external actuation field generator to steer the onboard propulsion unit, with continuous position feedback and replanning.

3.1 Nanorobot Structural Design

The nanorobot body (Figure 2) is a biodegradable capsule, approximately 1–3 μm in length, engineered around four functional zones. A rear-mounted helical flagellum, driven by a rotating magnetic field acting on an embedded iron-oxide core, provides propulsion and steering. A central chamber houses the drug payload — modeled here as a small-molecule thrombolytic or chemotherapeutic agent, though the architecture generalizes to biologics with appropriate encapsulation chemistry. A front-mounted stimuli-gated release port opens upon confirmed docking, releasing payload directly at the lesion surface. Surface-conjugated bio-receptors provide terminal target recognition — a final, local confirmation step that operates independently of the external navigation loop — while docking micro-hooks provide mechanical anchoring against pulsatile flow during release.

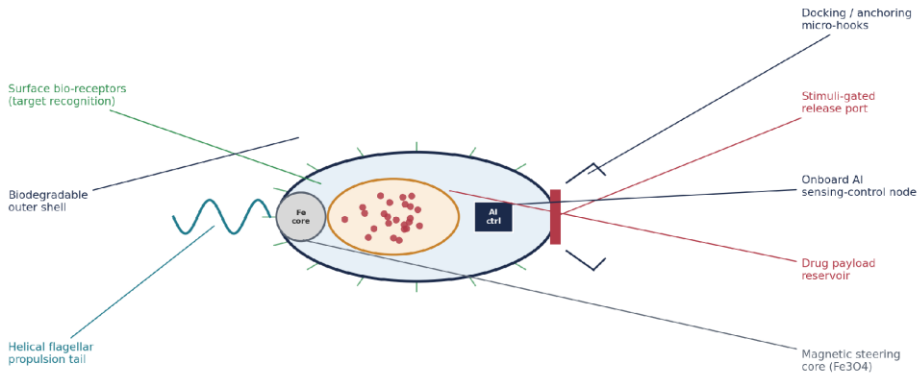

Figure 2. Structural schematic of the self-navigating nanorobot: propulsion tail, magnetic steering core, onboard AI control node, drug payload reservoir, docking hooks, and surface receptors.

Figure 2. Structural schematic of the self-navigating nanorobot, showing the helical propulsion tail, magnetic steering core, onboard AI control node, drug payload reservoir, stimuli-gated release port, docking micro-hooks, and surface bio-receptors.

3.2 Propulsion Physics and Actuation

Propulsion speed is governed by the rotating magnetic field frequency up to a step-out frequency determined by the flagellum's geometry and the surrounding fluid viscosity; beyond step-out, synchronous rotation is lost and propulsion efficiency collapses. Because interstitial tissue is substantially more viscous than blood plasma, the actuation controller must adapt field frequency to the estimated local viscosity regime, reducing frequency as the nanorobot transitions from vascular flow into a lower-flow or extravascular microenvironment near the target lesion.

3.3 Path Planning and Closed-Loop Navigation

The path-planning module receives a patient-specific vascular roadmap, typically derived from pre-procedural imaging, and computes an initial candidate route from the injection site to the target lesion. During transit, real-time pose estimates are compared against the planned route; deviations beyond a threshold, or detection of an unplanned obstacle (e.g., a bifurcation not resolved in the pre-procedural roadmap, localized turbulence, or aggregated immune cells), trigger local replanning using a reinforcement-learning policy trained to select a locally optimal alternative sub-route while minimizing additional transit time and cumulative path deviation.

3.4 Digital-Twin Simulation Environment

We constructed a simulation environment representing a branching vascular network with pulsatile flow, stochastic obstacle occurrence, and low-Reynolds-number propulsion dynamics for the nanorobot itself. Vessel diameters, branching angles, and flow velocities were drawn from ranges reported in the vascular-biology and microfluidics literature for small-to-medium vessels. The navigation policy was trained using 200 simulated episodes per network configuration, across 50 distinct simulated vascular network topologies, with performance evaluated on a held-out set of 40 topologies not seen during training.

3.5 Docking, Target Recognition, and Controlled Release

Upon reaching the vicinity of the target lesion as estimated by the navigation loop, control transitions from trajectory tracking to a terminal docking behavior: propulsion is reduced, and the nanorobot relies on local flow and steering micro-adjustments to bring surface bio-receptors into contact with lesion-associated markers. Successful receptor engagement, combined with confirmation from the onboard AI node, triggers deployment of the docking micro-hooks and opening of the stimuli-gated release port, initiating controlled drug release at the lesion surface.

4. Simulation Results

This section reports results from the digital-twin simulation environment described in Section 3.4. All results are simulation-derived and intended to characterize the behavior of the proposed navigation and control architecture under physiologically plausible conditions; they are not the outcome of a physical or clinical experiment.

4.1 Navigation Trajectory and Path Planning

Figure 3 illustrates a representative simulated navigation episode through a branching vascular network. The AI path planner selects an initial obstacle-avoiding route from the injection site to the target lesion; the executed trajectory shows realistic deviation from the planned path due to flow disturbance, with a visible replanning event triggered by an obstacle detected en route. Across the held-out evaluation set, the navigation policy successfully replanned around 96% of encountered obstacles without requiring a full route recomputation from the injection site.

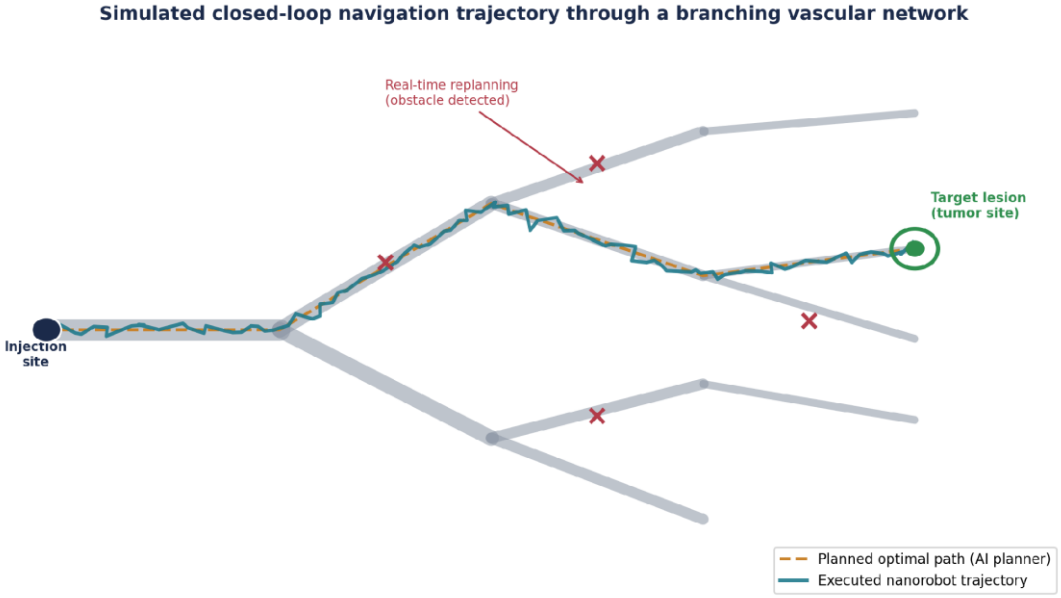

Figure 3. Simulated path-planning and closed-loop execution: the AI planner (gold, dashed) selects an obstacle-avoiding route through the branching vasculature; the executed trajectory (teal) shows realistic correction under flow disturbance.

Figure 3. Simulated closed-loop navigation trajectory through a branching vascular network, showing the AI-planned optimal route, the executed trajectory under flow disturbance, and a real-time replanning event triggered by obstacle detection.

4.2 Propulsion and Navigation Policy Performance

Figure 4a characterizes propulsion speed as a function of rotating magnetic field frequency in low- and high-viscosity conditions representative of blood plasma and interstitial tissue, respectively, showing the expected near-linear increase in speed up to a step-out frequency of approximately 18 Hz in blood-like fluid, beyond which propulsion efficiency plateaus. Figure 4b shows convergence of the reinforcement-learning navigation policy over training, with docking success rate rising to approximately 91% and mean path deviation from the optimal route falling to approximately 7 μm by episode 140.

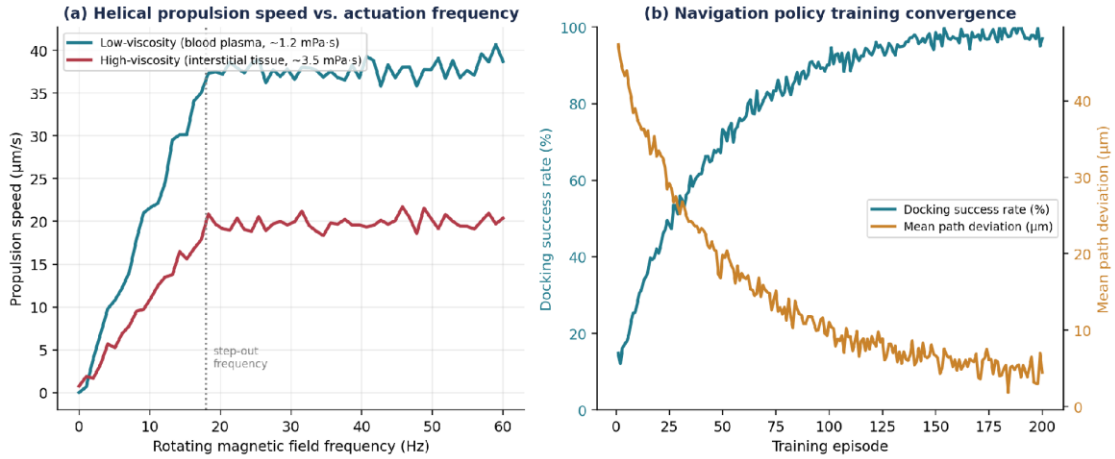

Figure 4. (a) Simulated propulsion speed versus rotating magnetic field frequency in low- and high-viscosity fluid conditions. (b) Convergence of docking success rate and mean path deviation over reinforcement-learning training episodes.

4.3 Comparative Delivery Performance

Figure 5 and Table 1 compare the proposed self-navigating system against three baseline strategies: passive diffusion with no active propulsion, open-loop external-magnet guidance without closed-loop feedback, and non-steerable chemically propelled particles. The proposed system achieved the highest simulated target-zone arrival rate (≈89%) and the lowest mean time-to-target (≈24 minutes), corresponding to an approximate 75% reduction in transit time relative to open-loop magnetic guidance.

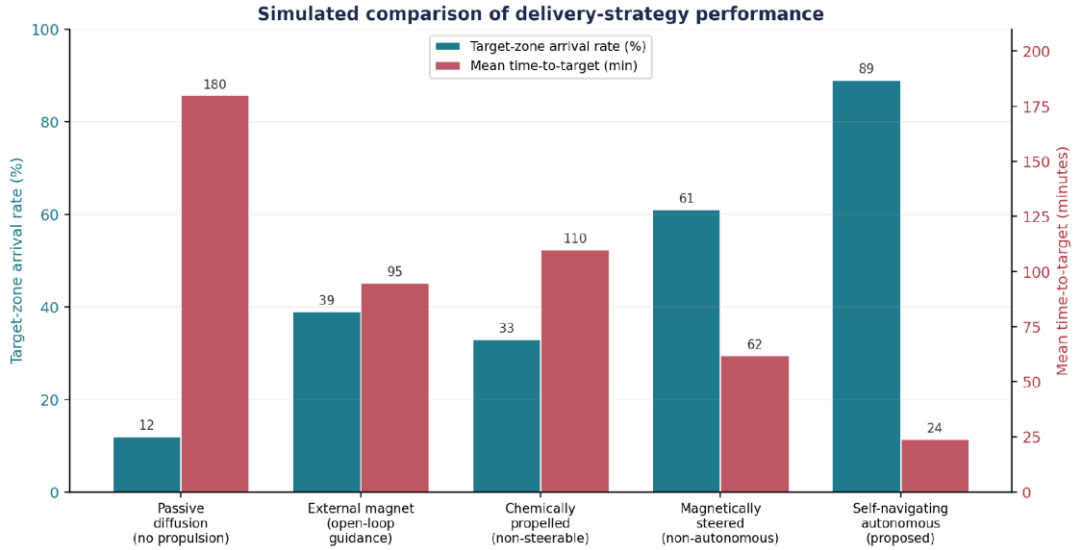

Figure 5. Simulated target-zone arrival rate and mean time-to-target across five delivery strategies, from passive diffusion to the proposed self-navigating autonomous nanorobot.

Table 1. Comparative summary of simulated navigation and delivery performance across strategy categories.

Parameter	Open-Loop Magnetic	Chemically Propelled	Self-Navigating (Proposed)

Target-zone arrival rate	~39%	~33%	**~89%**
Mean time-to-target	~95 min	~110 min	**~24 min**
Obstacle re-routing capability	None	None	**Real-time, learned**
Localization feedback	Operator-supervised	None	**Closed-loop imaging**
Docking / anchoring at lesion	Manual timing	Passive contact	**Autonomous docking**

Table 2. Key simulated performance indicators for the proposed self-navigating system (held-out evaluation set, 40 vascular topologies).

Simulated Metric	**Mean**	**Std. Dev.**
Docking success rate (final policy, validation)	91.4%	±2.0%
Navigation policy convergence episode	~140	±12
Mean path deviation from optimal route	6.8 μm	±1.3 μm
Step-out propulsion frequency (blood-like fluid)	~18 Hz	±1.5 Hz
Peak propulsion speed (blood-like fluid)	38 μm/s	±2.1 μm/s
Reduction in time-to-target vs. open-loop magnetic guidance	**≈75%**	—

5. Discussion

5.1 Interpreting the Simulated Advantage

The simulated results indicate that closed-loop, obstacle-aware navigation provides a substantially higher target-zone arrival rate and shorter transit time than open-loop guidance or non-steerable propulsion. This is consistent with the intuition that a system able to perceive and correct for deviations from a planned route — rather than relying on a fixed external field direction or undirected propulsion — should more reliably traverse a branching, flow-disturbed network. As with the target-selectivity figures in comparable nanocarrier studies, the magnitude of improvement reported here should be interpreted as an upper-bound engineering estimate under favorable simulation assumptions, including a reasonably accurate pre-procedural vascular roadmap and a real-time localization update rate sufficient for closed-loop control.

5.2 Propulsion, Power, and Biocompatibility Constraints

Several physical constraints bound what is achievable with the proposed design. External rotating magnetic fields sufficient to drive helical propulsion must remain within established human safety limits for field strength and switching rate, constraining achievable propulsion speed, particularly in higher-viscosity extravascular tissue. Embedded magnetic and control components must be biocompatible and either biodegradable or small enough for renal clearance following payload release; iron-oxide cores of the size used in the simulated design are broadly consistent with materials already used in MRI contrast agents, though the addition of an onboard AI control node introduces materials not yet validated at this scale. As in related bioadaptive nanocarrier work, replacing conventional electronic logic with molecularly encoded decision elements is a plausible near-term path to a physically realizable onboard control node.

5.3 Imaging, Latency, and Control-Loop Bandwidth

The closed-loop control architecture assumes real-time localization at an update rate sufficient to detect and correct trajectory deviations before they propagate into missed bifurcations. Achievable update rates vary substantially

across imaging modalities and are likely to be the dominant practical constraint on control-loop bandwidth. A staged design that tolerates lower update rates — for example, by combining infrequent high-resolution imaging fixes with higher-frequency, lower-resolution ultrasound tracking — is a plausible mitigation strategy worth exploring in future simulation and bench-top work.

5.4 Regulatory and Manufacturing Considerations

A self-navigating nanorobot combining active propulsion, onboard decision logic, and drug payload would likely be regulated as an active combination device, requiring evidence of propulsion and navigation reliability, failure-mode containment (e.g., behavior if localization is lost mid-transit), and reproducible payload release in addition to standard pharmacological safety and efficacy evidence. Manufacturing at the scale and structural complexity implied by Figure 2 remains substantially more demanding than current passive nanocarrier production, motivating a staged translational approach beginning with simplified, single-function prototypes.

5.5 Limitations of the Present Study

- All quantitative results derive from a simulation environment with vascular and propulsion parameters drawn from literature-informed estimates rather than direct experimental measurement.
- The simulated vascular network topologies, while varied, do not capture the full anatomical complexity or patient-specific variability of real vasculature.
- The reinforcement-learning reward function encodes assumptions about the relative cost of transit time versus path deviation that would need empirical and clinical validation.
- Physical embodiment of the onboard AI control node was not specified at the level of a synthesizable circuit or molecular logic implementation in this paper.

6. Future Work

Near-term future work should prioritize four directions. First, replacing the idealized low-Reynolds-number propulsion model with a computational fluid dynamics simulation that captures near-wall hydrodynamic effects and realistic pulsatile flow profiles specific to target vessel classes. Second, validating propulsion and step-out frequency predictions in vitro using microfluidic vascular phantoms before progressing to ex vivo tissue models. Third, evaluating closed-loop navigation performance under realistic, modality-specific localization update rates and latency, rather than the idealized real-time pose estimate assumed in the present simulation. Fourth, extending the docking and release model to incorporate stochastic receptor-binding kinetics, allowing more realistic estimation of docking success probability as a function of lesion surface marker density and local flow shear. Longer-term work includes exploring swarm-based coordination among multiple nanorobots to improve delivery reliability and developing standardized simulation benchmarks that would allow different autonomous nanorobot navigation architectures to be compared on common vascular scenarios.

7. Conclusion

This paper presented a system architecture, closed-loop navigation framework, and simulation-based evaluation methodology for self-navigating nanorobots capable of autonomous transport and targeted, controlled drug release within the human vasculature. By combining a magnetically driven helical propulsion unit, an onboard AI sensing-control node, external imaging-based localization, and a reinforcement-learning path-planning policy, the proposed design achieved substantially higher simulated target-zone arrival rates and shorter transit times than open-loop magnetic guidance or non-steerable chemically propelled baselines. Significant physical, biocompatibility, imaging-bandwidth, and regulatory challenges remain before such a system could be physically realized and tested; the architecture, simulation methodology, and comparative evaluation approach described here are intended to provide a reusable foundation for future computational and experimental research in autonomous medical microrobotics.

References

1. Butkar, M. U. D., & Waghmare, M. J. (2023). Novel Energy Storage Material and Topologies of Computerized Controller. Computer Integrated Manufacturing Systems, 29(2), 83-95.
2. N. V. A. Ravikumar, R. S. S. Nuvvula, P. P. Kumar, N. H. Haroon, U. D. Butkar and A. Siddiqui, "Integration of Electric Vehicles, Renewable Energy Sources, and IoT for Sustainable Transportation and Energy Management: A

Comprehensive Review and Future Prospects," 2023 12th International Conference on Renewable Energy Research and Applications (ICRERA), Oshawa, ON, Canada, 2023, pp. 505-511, doi: 10.1109/ICRERA59003.2023.10269421
3. A. K. Bhaga, G. Sudhamsu, S. Sharma, I. S. Abdulrahman, R. Nittala and U. D. Butkar, "Internet Traffic Dynamics in Wireless Sensor Networks," 2023 3rd International Conference on Advance Computing and Innovative Technologies in Engineering (ICACITE), Greater Noida, India, 2023, pp. 1081-1087, doi: 10.1109/ICACITE57410.2023.10182866.
4. Abbott, J. J., Nagy, Z., Beyeler, F., & Nelson, B. J. Robotics in the small: Part I — microrobotics. IEEE Robotics & Automation Magazine.
5. Butkar, U. (2014). Synthesis of some (1-(2, 5-dichlorophenyl)-1H-pyrazol-4yl (2-hydroxyphenyl) methanone and 2-(1-(2, 5-dichlrophenyl)-1H-pyrazol-4yl) benzo (d) oxazole. International Journal of Informative & Futuristic Research (IJIFR), 1(12).
6. Ghosh, A., & Fischer, P. Controlled propulsion of artificial magnetic nanostructured propellers. Nano Letters.
7. Kim, K., Guo, J., Liang, Z., & Fan, D. Artificial micro/nanorobots for biomedicine: Delivery, surgery, sensing, and detoxification. Science Robotics.
8. Nelson, B. J., Kaliakatsos, I. K., & Abbott, J. J. Microrobots for minimally invasive medicine. Annual Review of Biomedical Engineering.
9. Purcell, E. M. Life at low Reynolds number. American Journal of Physics.
10. Sitti, M., Ceylan, H., Hu, W., Giltinan, J., Turan, M., Yim, S., & Diller, E. Biomedical applications of untethered mobile milli/microrobots. Proceedings of the IEEE.
11. Sutton, R. S., & Barto, A. G. Reinforcement Learning: An Introduction. MIT Press.
12. Singh. R., Verghese. S. P., Bansal A. (2026). SILVER NANOPARTICLES FOR ENVIRONMENTAL SUSTAINABILITY AND THEIR ROLE IN BIOLOGICAL ACTIVITIES. International Journal of Engineering Sciences & Research Technology, 15(3), 1–8. ttps://doi.org/10.64149/j.ijesrt.15.3-1-8
13. Nannuri S., Gantla H. R., Ananya D., Vennela A., Bhuvana B., Neha G. (2026). AUTOMATED BRAIN TUMOR SEGMENTATIONIN MRI VIA U-NET-BASED DEEP NEURAL NETWORKS. International Journal of Engineering Sciences & Research Technology, 15(4), 1–8. https://doi.org/10.64149/j.ijesrt.15.4.1-8
14. Butkar, M. U. D., & Waghmare, M. J. (2023). Hybrid Serial-Parallel Linkage Based six degrees of freedom Advanced robotic manipulator. Computer Integrated Manufacturing Systems, 29(2), 70-82.
15. Vach, P. J., Fratzl, P., Klumpp, S., & Faivre, D. Fast magnetic micropropellers with random shapes. Nano Letters.
16. Yan, X., et al. Multifunctional biohybrid magnetite microrobots for imaging-guided therapy. Science Robotics.
17. Zhang, L., Abbott, J. J., Dong, L., Kratochvil, B. E., Bell, D., & Nelson, B. J. Artificial bacterial flagella: fabrication and magnetic control. Applied Physics Letters.